Section S1 Experimental.

1. Materials

Sodium nitroprusside ($C_5H_4FeN_6Na_2O_3$, 99.98%), salicylic acid ($C_7H_6O_3$, 99.5%), and sodium hypochlorite (NaClO, 6-14% active chlorine basis) were purchased fromRon Reagent. Trisodium citrate ($C_6H_5O_7Na_3 \cdot H_2O$, ≥99.5%) was obtained from Tianjin Damao Chemical Trading Co., Ltd. NaOH (96%) were purchased from Tianjin Kermel Chemical Reagent Co., Ltd. Acetone (CH_3COCH_3, 99.5%) was obtained from Tianjin Wind Ship Chemical Reagent Co., Ltd. Anhydrous sodium sulfate (Na_2SO_4, 99%), ascorbic acid (AA, > 99.0%), chloric acid (Au 23.5 ~ 23.8% in dilute HCl), ammonium chloride (NH_4Cl, 99.99%), $Zn(NO_3)_2 \cdot 6H_2O$ (≥ 99.5%), 2-methylimidazole (≥ 99.5%), $Na^{15}NO_3$ (99atom%) and $^{15}NH_4Cl$ (99atom%) were obtained from Aladdin. Methyl alcohol (CH_3OH, 99.7%), anhydrous ethanol (CH_3CH_2OH, 99.7%) was purchased from Shandong Bocheng Chemical Co., Ltd. Polyethylene pyrrolidone (PVP, average M.W. = 130,000, 99%) was from Shanghai Yuanye Bio-Technology Co., Ltd. Chloroplatinic acid hexahydrate ($H_2PtCl_6 \cdot 6H_2O$, Pt ≥ 37.5%), and paradimethylaminobenzaldehyde ($C_9H_{11}NO$) were obtained from Maclin. Hydrazine hydrate (N_2H_4, 5% HCl) was obtained from Guobiao (Beijing) Testing and Certification, Co., Ltd. Silver nitrate ($AgNO_3$, ≥ 99.5%) was obtained from Boort (Tianjin) Chemical Trading Co., Ltd. All chemical reagents were used without further purification.

Transmission electron microscopy (TEM) imagings were performed on a Philips Tecnai F20 system at 200 kV to observe the morphology and analyze the elements quantitatively and qualitatively by EDS mapping. Powder X-ray diffraction (XRD) patterns were recorded on Bruker GADDS XRD diffractometer with Cu K_α radiation to obtain the structures of composites. The chemical composition and bonding characteristics were analyzed by X-ray photoelectron spectroscopy (XPS) of PHI Quantera under monochromatic Mg X-ray radiation source. ^1H NMR spectra were recorded on a Bruker NMR spectrometer (400 MHz) with chemical shifts reported as

ppm in DMSO-d6. NO_3RR tests were conducted using a CHI760E electrochemical workstation.

2. Synthesis

Synthesis of pAu. A one-step synthesis strategy was used to synthesize porous Au structure (pAu). In general, pAu were prepared in the presence of Ag^+ using hydroquinone as the reducing agent, $HAuCl_4$ as the precursor, and polyvinylpyrrolidone (PVP) as the surfactant. Then the AgCl templates were removed by the dealloying method to obtain pAu particles. Firstly, 320 μL of 28 mM hydroquinone solution, 60 μL of 10 mM $AgNO_3$ solution, and 6.3 μL of $HAuCl_4$ solution were added to 4.5 mL of 90 mM PVP solution. Then the mixture is kept under gentle stirring for 3 minutes at room temperature and a steady state for 30 minutes. The solution was then washed with ammonia to etch the template AgCl, further purified with acetone, ethanol, methanol and repeated centrifugation.

Synthesis of porous AuPt. Typically, 2.3 mL of pAu solution at a concentration of 0.25 mg/mL was added to a vial containing 5 mL of water; then a volume of H_2PtCl_6 solution (1mM) was added. After stirring at 700 rpm for 1 hour, a calculated amount of ascorbic acid (0.2M) was added to the vial at 700 rpm with stirring; the volume ratio of H_2PtCl_6 solution to ascorbic acid solution was fixed at 1:1 (118 μL:118 μL). After mixing for 10 minutes, the mixture was heated at 50 ℃ for 14 h. The final products were centrifuged, washed, and dispersed in ethanol.

Synthesis of AuPt@ZIF-8. 5-mg porous AuPt alloys were dispersed in 1-mL ethanol. AuPt solution (8 μL, 5 mg/mL) was dropped on the surface of the polished glassy carbon electrode and naturally dried at room temperature. The electrode is immersed in the solution containing zinc nitrate (2.5 mL, 25 mM) and 2-methylimidazole (2.5 mL, 25 mM). The electrodes were rinsed several times with methanol after 50 minutes.

3. NO_3RR measurement

For NO_3RR electrochemical testing, a gas-tight, two-compartment cell separated

by a Nafion membrane was used for evaluation. The working electrode and the Ag/AgCl reference electrode were placed in the cathode chamber. In the anode chamber, a Pt sheet was used as the counter electrode. Before the experiment, the membrane was boiled in ultrapure water for 1-hour, treated in H_2O_2 (5%) aqueous solution at 80 ℃ for 1 hour. Then, the membrane was soaked in 0.5 M H_2SO_4 for 2 hours at 80 ℃, and subsequently boiled in water for 6 hours. AuPt@ZIF-8 was used as the working electrode with Ag/AgCl as the reference electrode, and Pt sheet as the counter electrode for electrolysis in an electrolytic cell. The electrolyte is composed of 0.1 M Na_2SO_4 and 50 ppm $NaNO_3$ with pH of 7.66. Before each electrochemical test, Ar gas was continuously fed into the electrolyte for at least 1 hour. The constant and stable access of Ar is maintained during the electrolysis. All given potentials were converted to reversible hydrogen electrode potential by E (vs RHE) = E (vs Ag/AgCl) + 0.059 pH + 0.197 V. Electrochemical test was performed for 1 hour at the applied potentials of − 0.50 V, − 0.55 V, − 0.60 V, − 0.65 V and − 0.70 V vs RHE. The control experiments for the verification of ammonia origin involves the electrochemical CA tests (a) with the same AuPt@ZIF-8 working electrode in the electrolyte of 0.1 M Na_2SO_4 without $NaNO_3$; (b) with the unfunctionalized glassy carbon working electrode in the same electrolyte of 0.1 M Na_2SO_4 and 50 ppm $NaNO_3$.

4. Detection of ammonia

Ammonia in the electrolyte was quantified after 1-h electrolysis by indophenol blue method. Firstly, the color reagent system were prepared. Solution A: 1 M NaOH solution (containing 5% salicylic acid and 5% sodium citrate); solution B: 0.05 M NaClO solution; solution C: 1 wt% $C_5FeN_6Na_2O$ (sodium nitroferricyanide) aqueous solution. 2 mL of electrolyte was mixed with 2-mL solution A, 1-mL solution B and 0.2-mL solution C evenly, and the reaction was kept for 2 hours at room temperature. The absorbance at 655 nm was recorded by using UV-Vis absorption spectrometer. Then NH_4Cl standard solution with a series of different concentrations was configured for UV-Vis tests and the standard curve of indophenol blue method was

established to calculate the ammonia amount. The ammonia concentration in the electrolyte was calculated by the linear equations.

5. Detection of by-product material

The by-product N_2H_4 in the electrolyte was quantified by Watt-Chrisp method after 1-hour electrolysis. Firstly, the color reagent system was prepared. P-dimethylaminated benzaldehyde (5.99 mg) was dissolved in a mixture of absolute ethanol (300 mL) and concentrated hydrochloric acid (30 mL). 5 mL of chromogen was mixed with 5 mL of electrolyte and kept at room temperature for 20 minutes. The absorbance at 455 nm was recorded by using a UV-Vis absorption spectrometer. Then, a series of concentrations of N_2H_4 standard solution was tested by UV-Vis to establish the standard curve of N_2H_4. The hydrazine concentration in the electrolyte was calculated by the linear equations.

The by-product nitrite in the electrolyte was quantified after 1-h electrolysis by Watt-Chrisp method. Firstly, Griess reagent was prepared from 0.1 g N-(1-naphthyl) ethylenediamine dihydrochloride, 1.0 g sulfonamide and 2.94 mL H_3PO_4 dissolved in 50 mL deionized water. Then, 1.0-mL Griess reagent was mixed with 1.0-mL electrolyte and 2.0-mL H_2O and reacted at room temperature for 10 minutes, where sulfanilamide reacted with NO_2^- to form a diazo salt and then further reacted with the amine to form an azo dye. Next, a series of concentrations of standard solutions were prepared, and the absorbance at 540 nm was measured by UV-Vis to quantify the concentration of NO_2^-.

6. Calculation of ammonia yield rate, Faradaic efficiency and Selectivity

The performance of NO_3RR catalysts mainly depends on their high catalytic activity, high selectivity and excellent stability. The high catalytic activity can be measured by the Faradaic efficiency and the ammonia production rate. Faradaic efficiency (*FE*) refers to the ratio of the charge consumed in the electrocatalytic ammonia synthesis to the total charge passing through the electrode, which can be calculated according to the following equation:

$$FE = \frac{8 \times F \times C_{NH_3} \times V}{17 \times Q}$$

The ammonia production rate can be calculated by using the following equation:

$$v_{NH3} = \frac{C_{NH_3} \times V}{t \times m_{cat.}}$$

where F is Faradaic constant, C_{NH3} is the ammonia concentration determined by indophenol blue method, V is the electrolyte volume of NO_3RR, Q is the quantity of applied electricity, t is the time of electrochemical reaction, and $m_{cat.}$ is the catalyst mass used to functionalize glassy carbon electrode.

The selectivity can be calculated by the following equation:

$$Selectivity(\%) = \frac{v_{NH_3}}{v_{NH_3} + v_{NO_2^-} + v_{N_2H_4}} \times 100\%$$

where v_{NH_3} is ammonia yield, $v_{NO_2^-}$ is nitrite yield, and $v_{N_2H_4}$ is hydrazine yield.

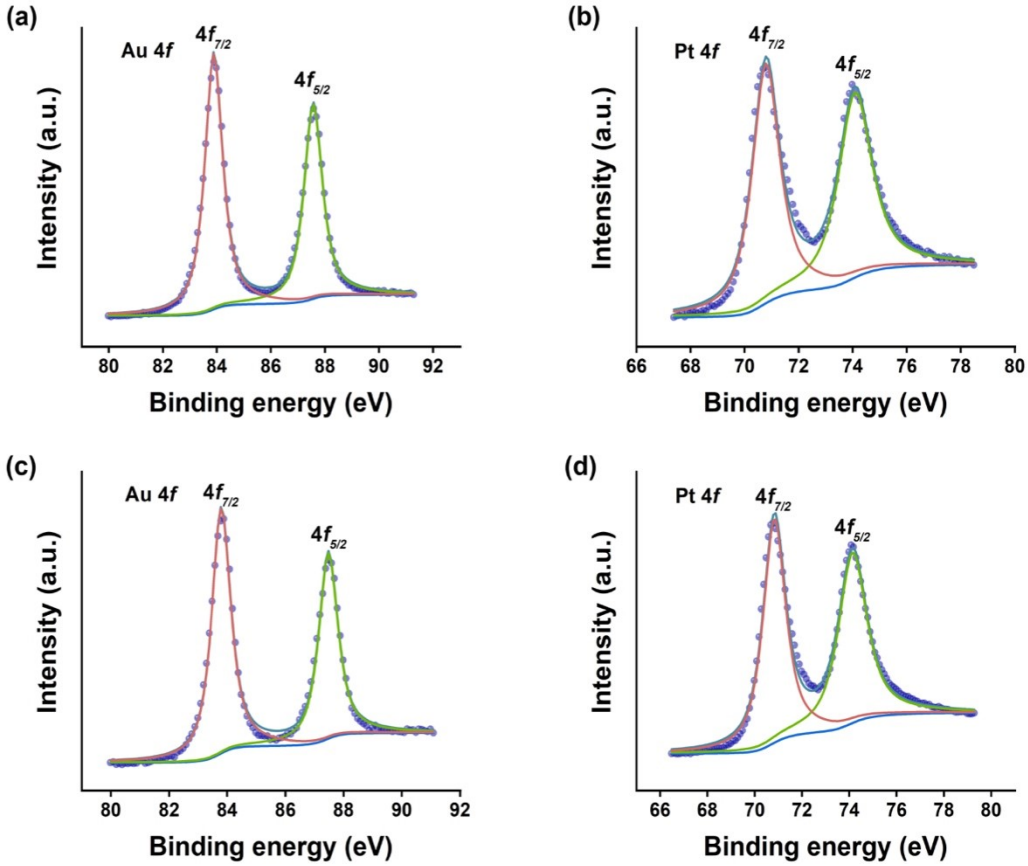

Figure S1. XPS at (a) Au 4*f*, (b) Pt 4*f* binding energy windows for 1% Pt of AuPt. XPS at (c) Au 4*f*, (d) Pt 4*f* binding energy windows for 3% Pt of AuPt. As for different Pt precursor ratios, all samples demonstrate the characteristic doublets of metallic Au at 83.8, 87.5 eV, and metallic Pt at 70.9, 74.2 eV.

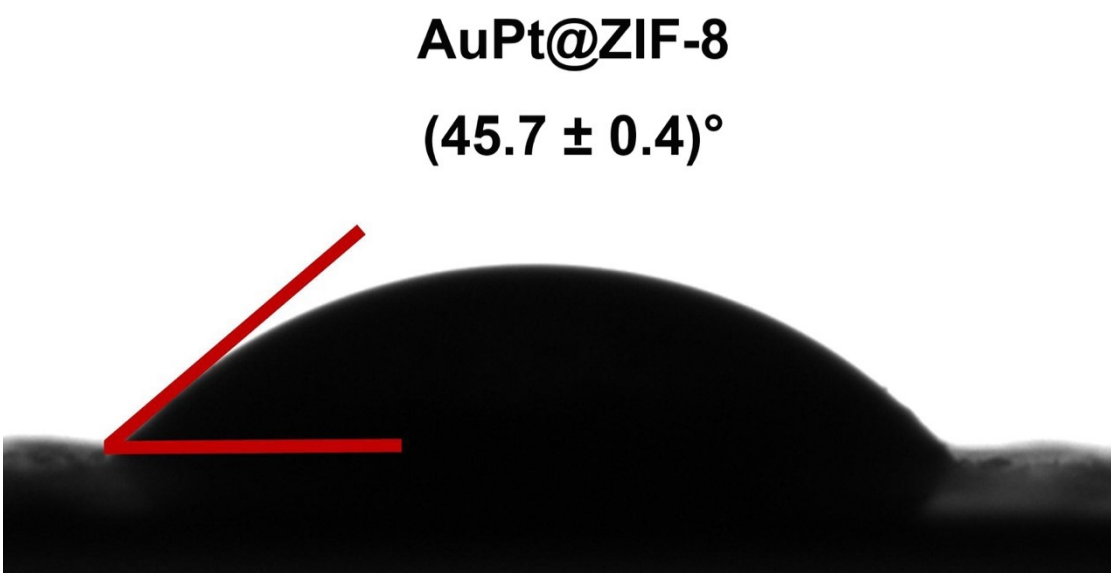

Figure S2. The static contact angle tests of AuPt@ZIF-8 using NO_3^- solution.

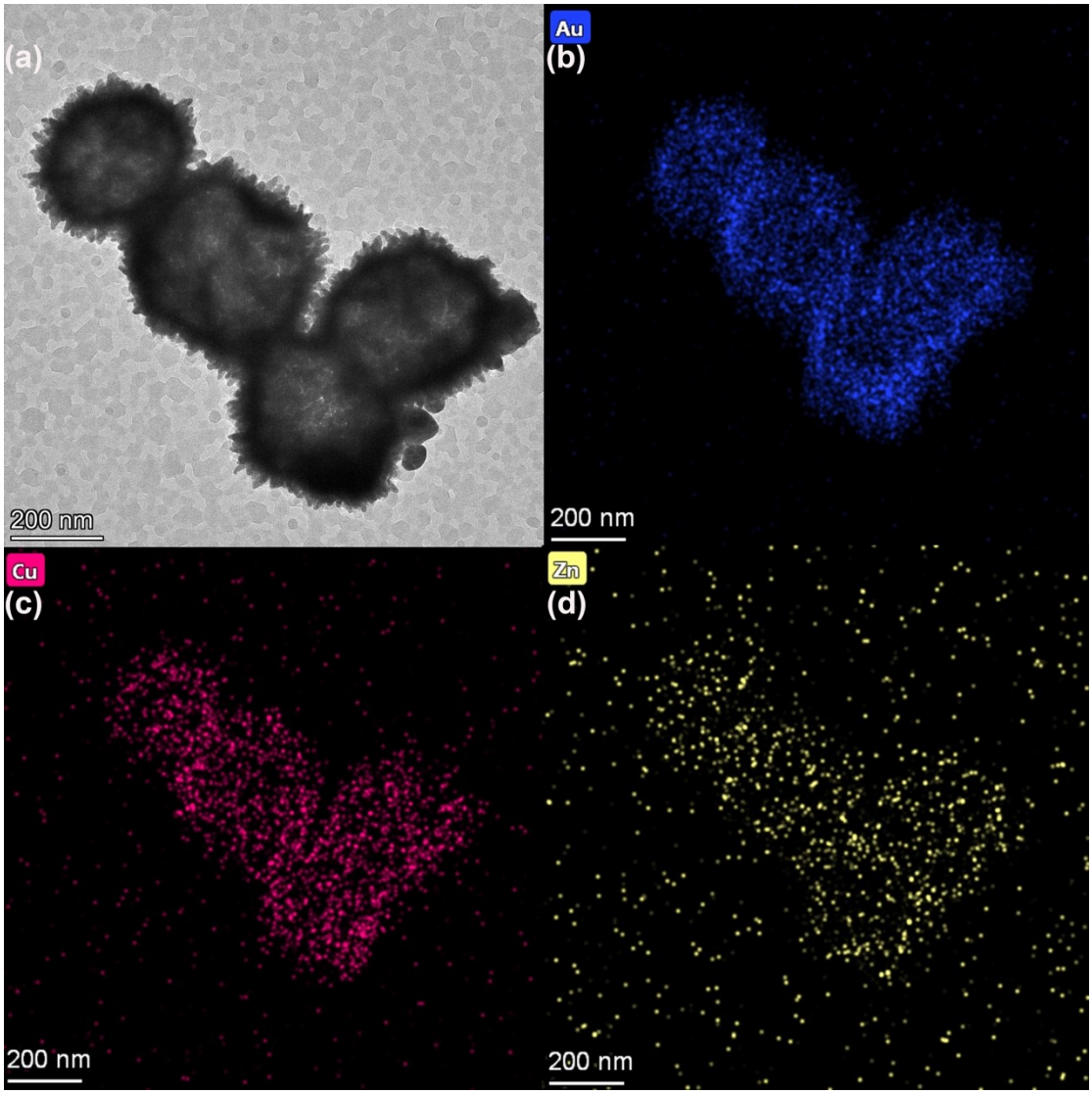

Figure S3. (a) Morphological characterization of the AuCu@ZIF-8 in the TEM image (scale bar: 200 nm). The porous AuCu particles display a spherical morphology and exhibit interconnected pores. EDS elemental mapping of (b) Au, (c) Cu and (d) Zn elemental distribution. Elemental composition of AuCu is 46.1:53.9 for Au:Cu. And the Au: Cu: Zn atomic ratio of AuCu@ZIF-8 is 72:25.5:2.5.

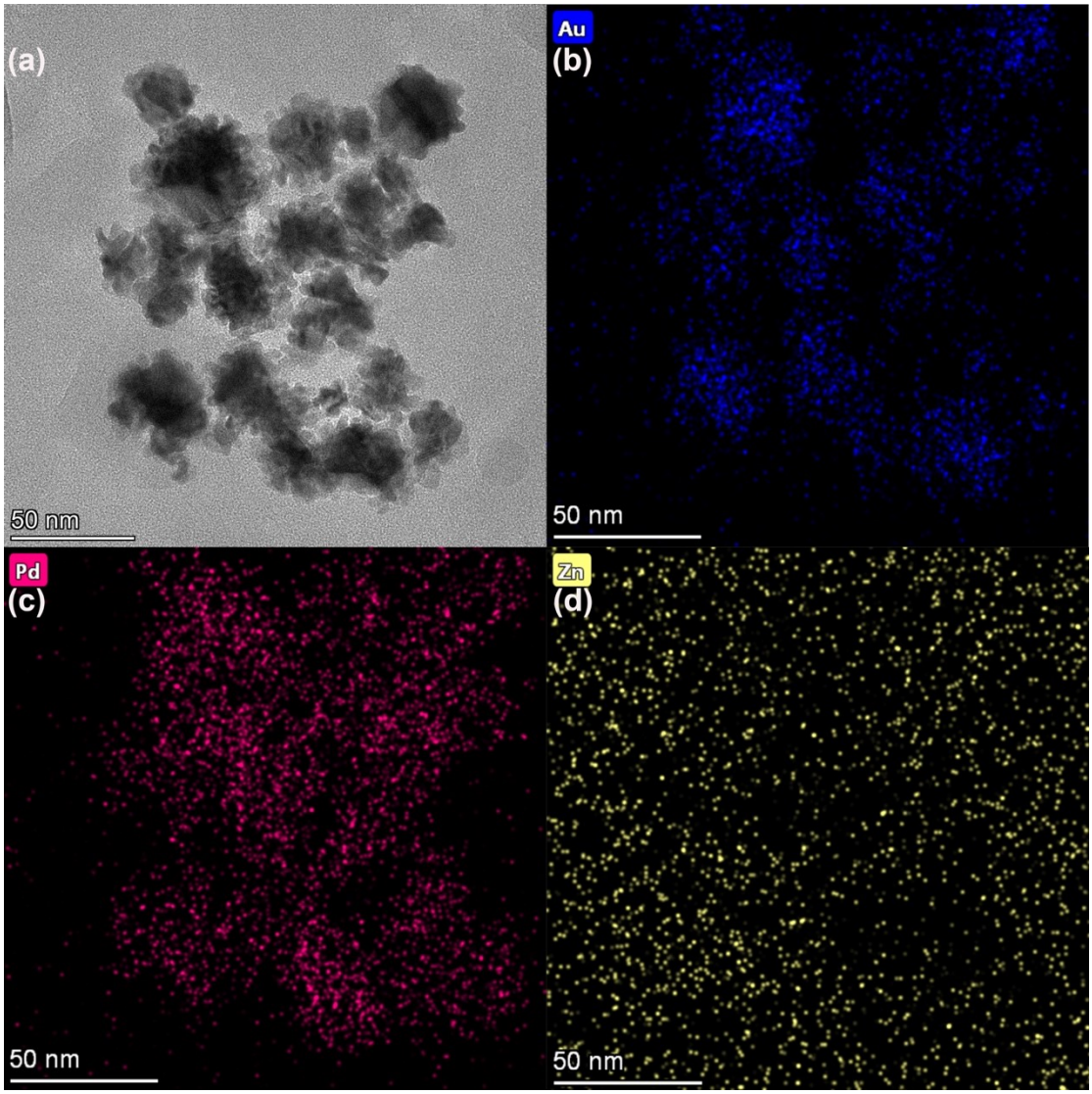

Figure S4. (a) Morphological characterization of the AuPd@ZIF-8 in the TEM image (scale bar: 50 nm). The porous AuPd particles exhibit a spherical morphology and each nanostructure exhibits porous properties with highly branched substituents, generating perpendicular pore channels between neighboring branches. EDS elemental mapping of (b) Au, (c) Pd and (d) Zn elemental distribution. Elemental composition is 44.0:56.0 for Au:Pd for AuPd. And the Au: Pd: Zn atomic ratio of AuPd@ZIF-8 is 27:33:40.

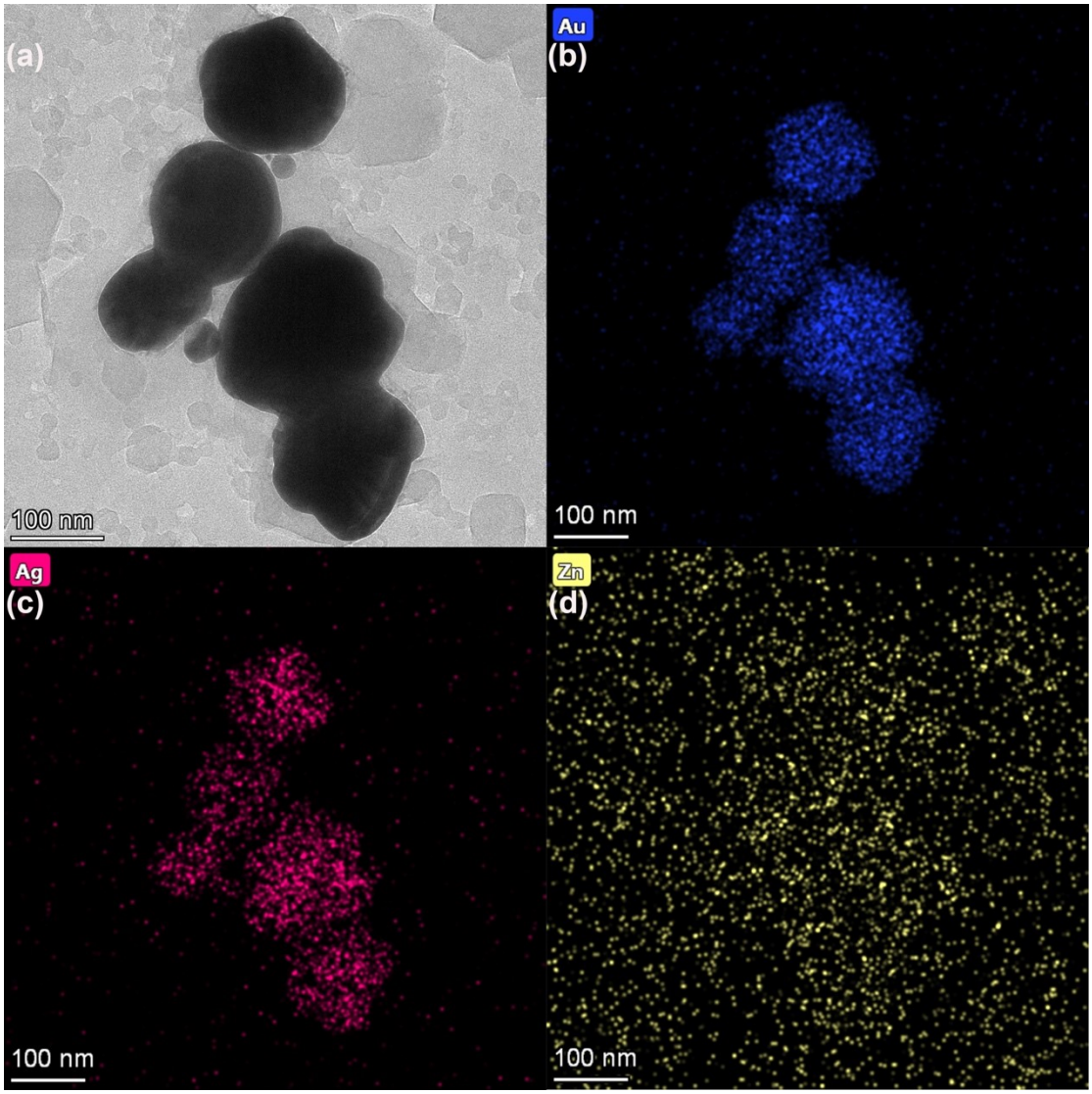

Figure S5. (a) Morphological characterization in the AuAg@ZIF-8 in the TEM image (scale bar: 100 nm). The AuAg particles exhibit a spherical morphology with an internal porous structure. EDS elemental mapping of (b) Au, (c) Ag and (d) Zn elemental distribution. Elemental composition of AuAg is 78.2:21.8. And the Au: Ag: Zn atomic ratio of AuAg@ZIF-8 is 68:13:19.

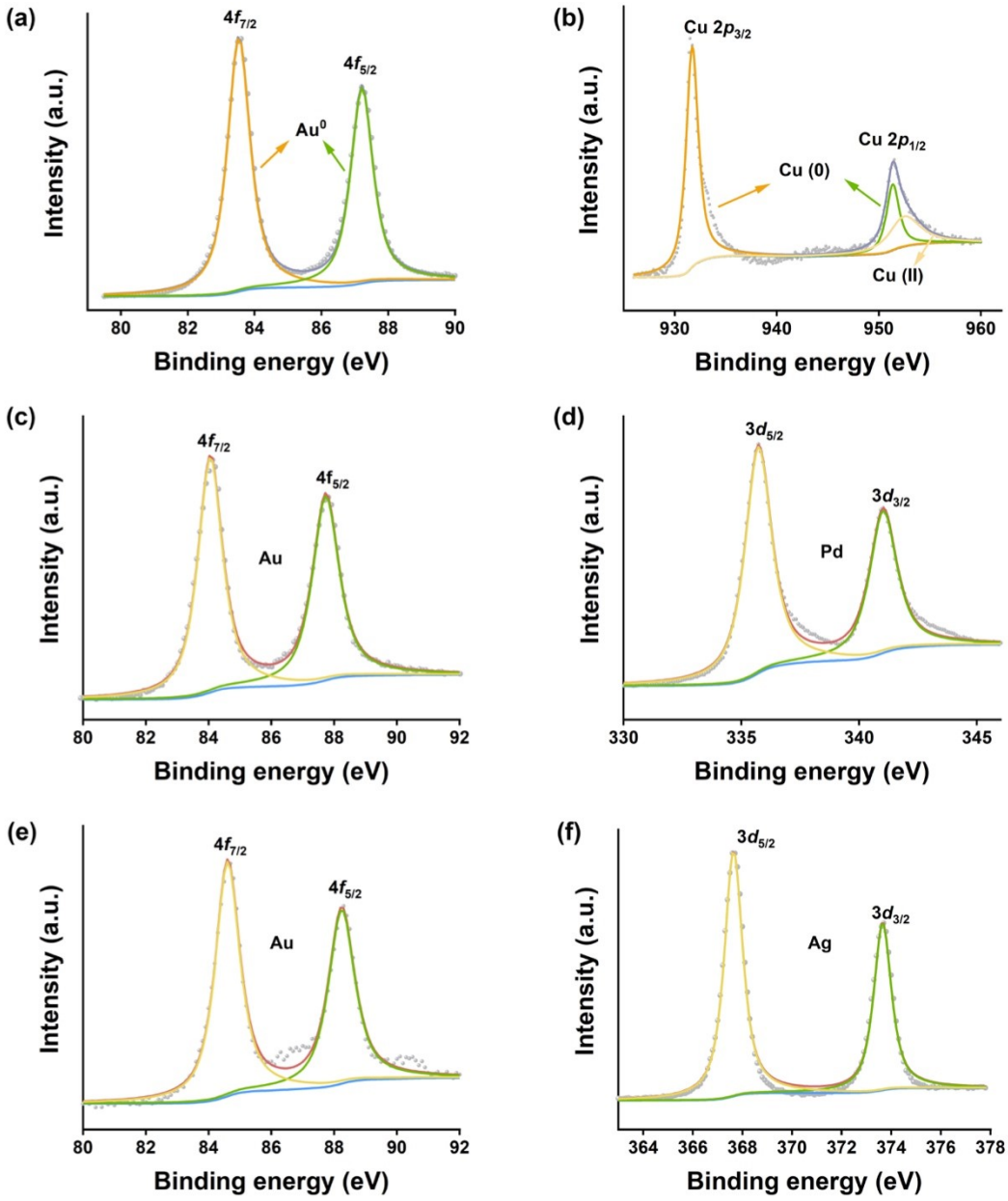

Figure S6. XPS at (a) Au 4*f*, (b) Cu 2*p* binding energy windows for AuCu, (c) Au 4*f*, (d) Pd 3*d* binding energy windows for AuPd, (e) Au 4*f*, (f) Ag 3*d* binding energy windows for AuAg. XPS patterns state the elemental valence of the corresponding metal with the ratio of 0.50:0.22 for Au:Cu, 1.2:6.5 for Au:Pd, 1.4:6.6 for Au:Ag

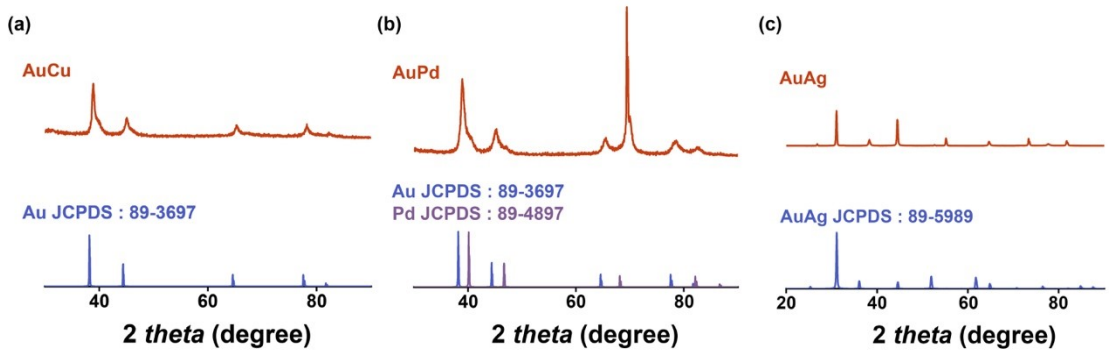

Figure S7. XRD patterns of porous (a) AuCu, (b) AuPd, (c) AuAg. XRD spectra also indicate the successful fabrication of porous AuCu, AuPd, AgAg and their composites.

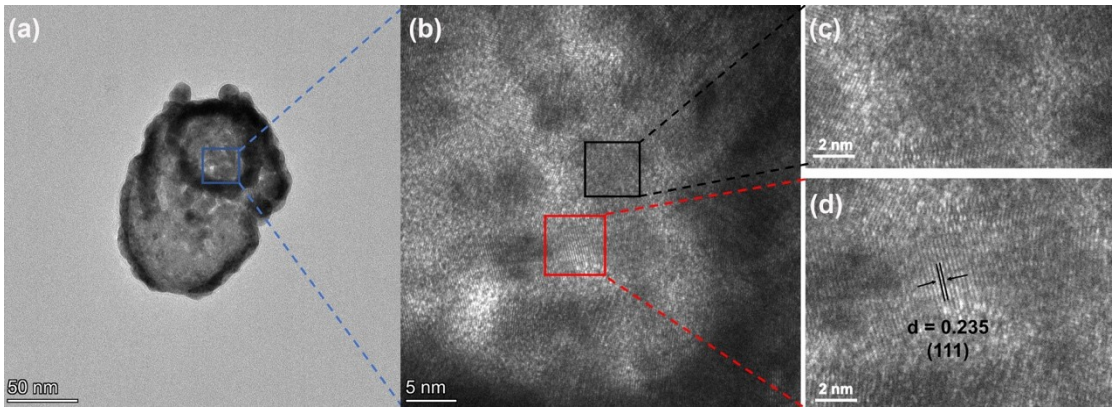

Figure S8. (a) TEM image of AuCu and (b-d) high-resolution TEM image in the square area. The lattice structure of Au shows plane spacing of 0.235 nm, which is indexed to the (111) lattice plane. No obvious XRD pattern for Cu in AuCu is resulted from amorphous Cu which is also proved by HRTEM.

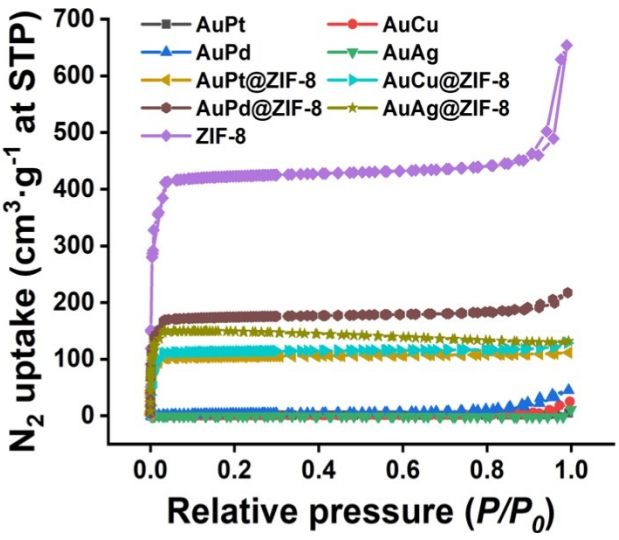

Figure S9. Nitrogen-sorption isotherms of AuPt, AuPt@ZIF-8, and other metal alloy structures at 77 K.

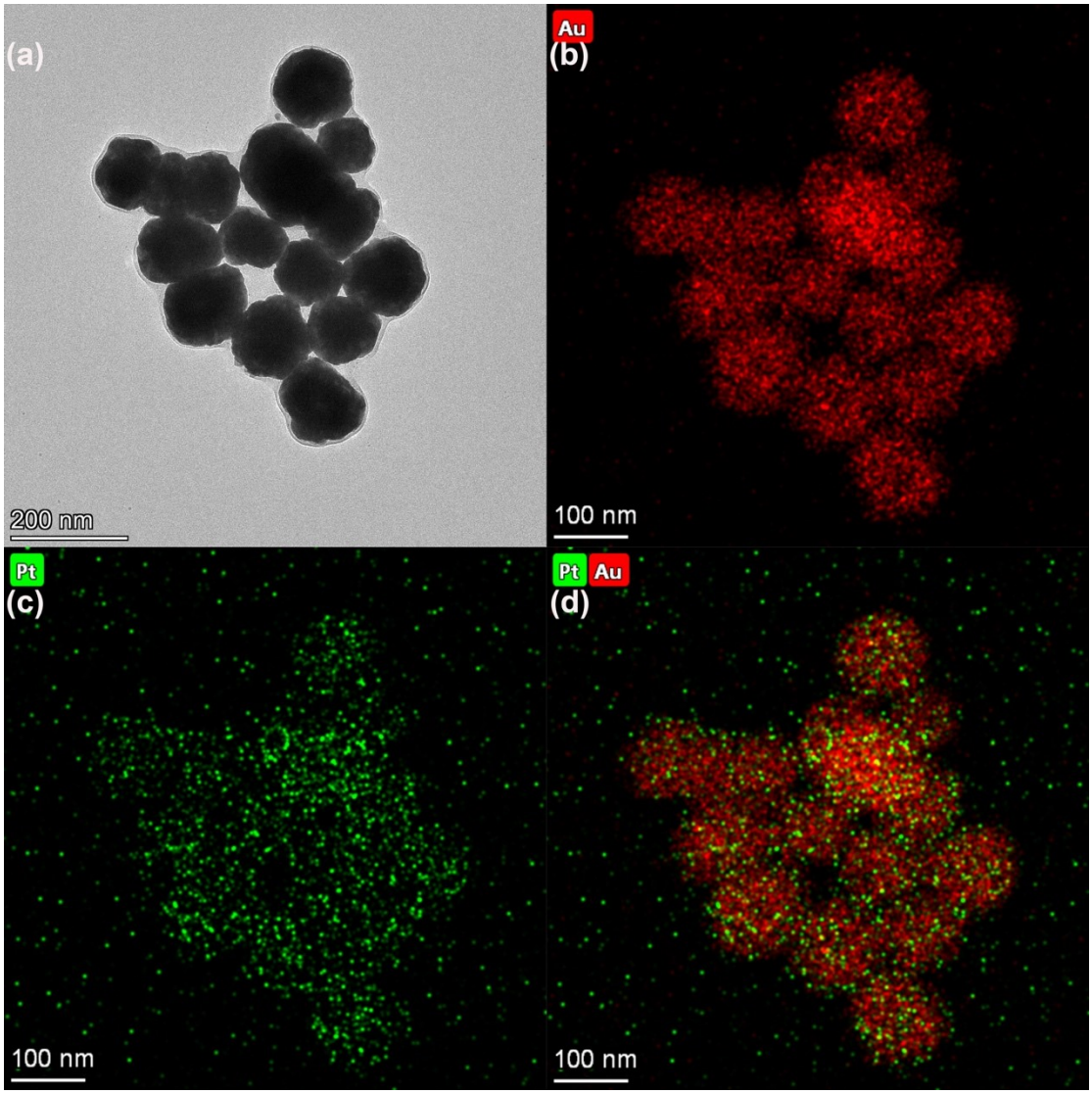

Figure S10. (a) Morphological characterization of the 1% Pt of AuPt in the TEM image (scale bar: 200 nm). EDS elemental mapping of (b) Au, (c) Pt and (d) AuPt elemental distribution. The Au: Pt atomic ratio of 1% Pt of AuPt is 99:1.

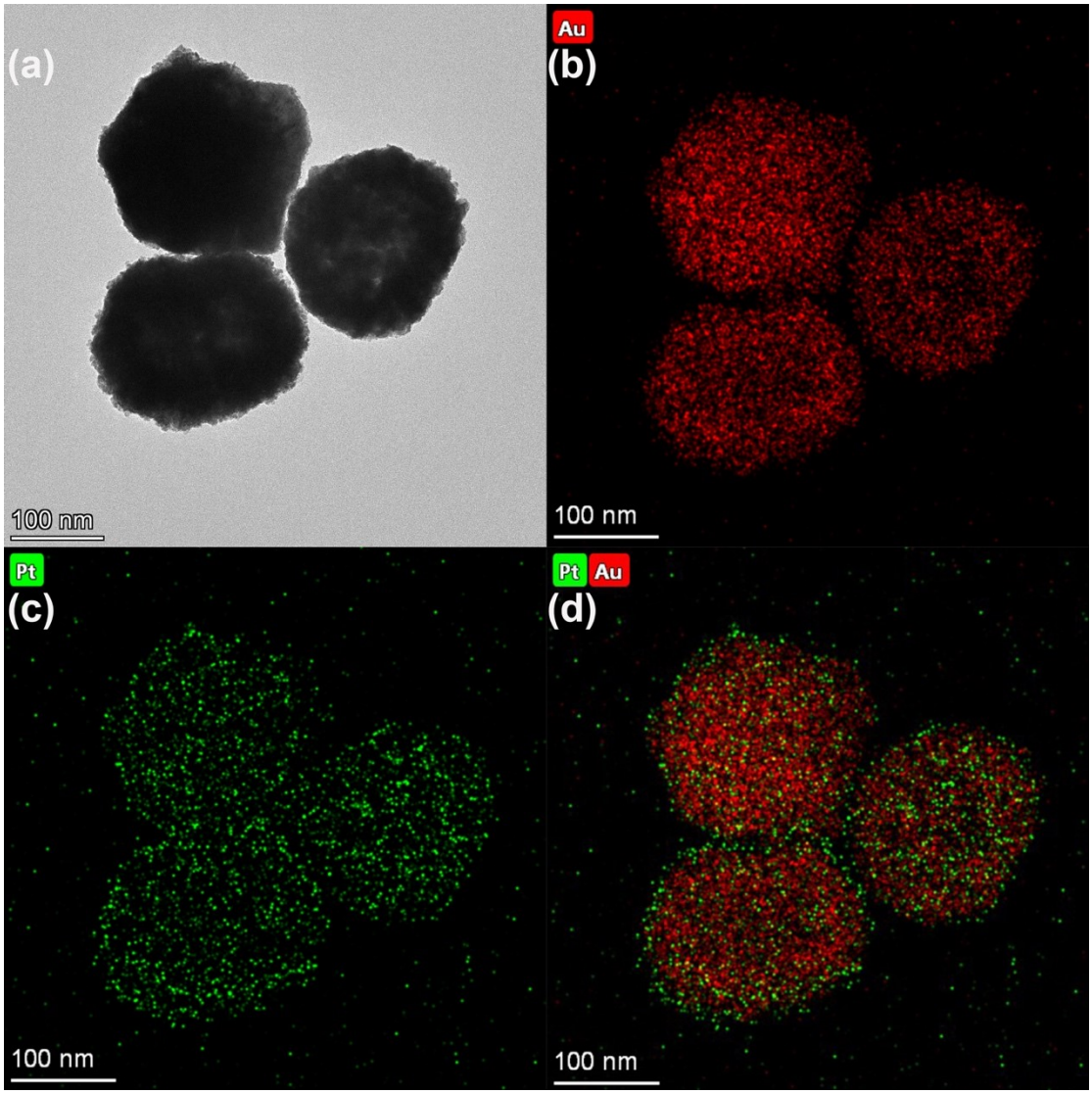

Figure S11. (a) Morphological characterization of the 3% Pt of AuPt in the TEM image (scale bar: 100 nm). EDS elemental mapping of (b) Au, (c) Pt and (d) AuPt elemental distribution. The Au: Pt atomic ratio of 3% Pt of AuPt is 96.9:3.1.

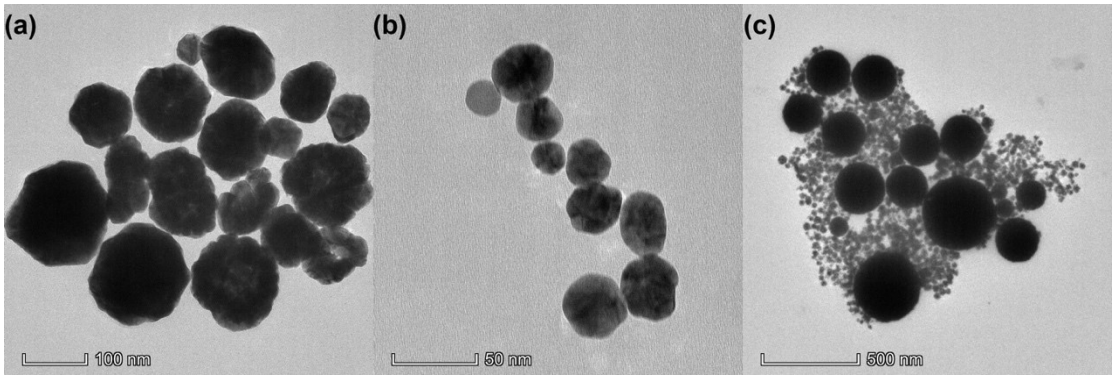

Figure S12. (a) Morphological characterization of the pAu in the TEM image (scale bar: 100 nm). (b) Morphological characterization of the solid Au in the TEM image (scale bar: 50 nm). (c) Morphological characterization in the solid Pt in the TEM image (scale bar: 500 nm).

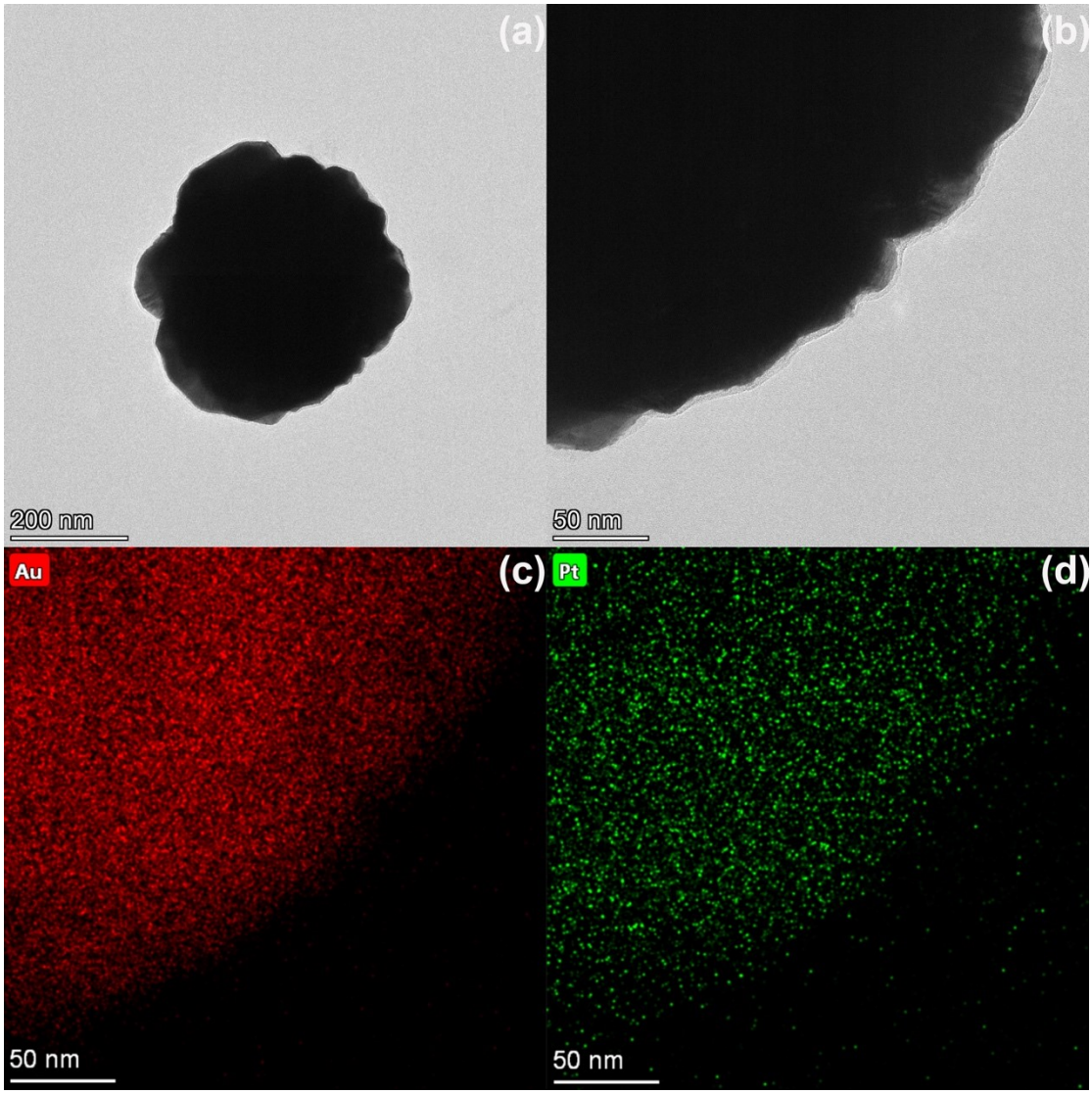

Figure S13. (a) Morphological characterization and magnified image of 1% Pt of AuPt (scale bar: 200 nm; 50 nm). EDS elemental mapping of (c) the Au and (d) Pt elemental distribution (scale bar: 50 nm).

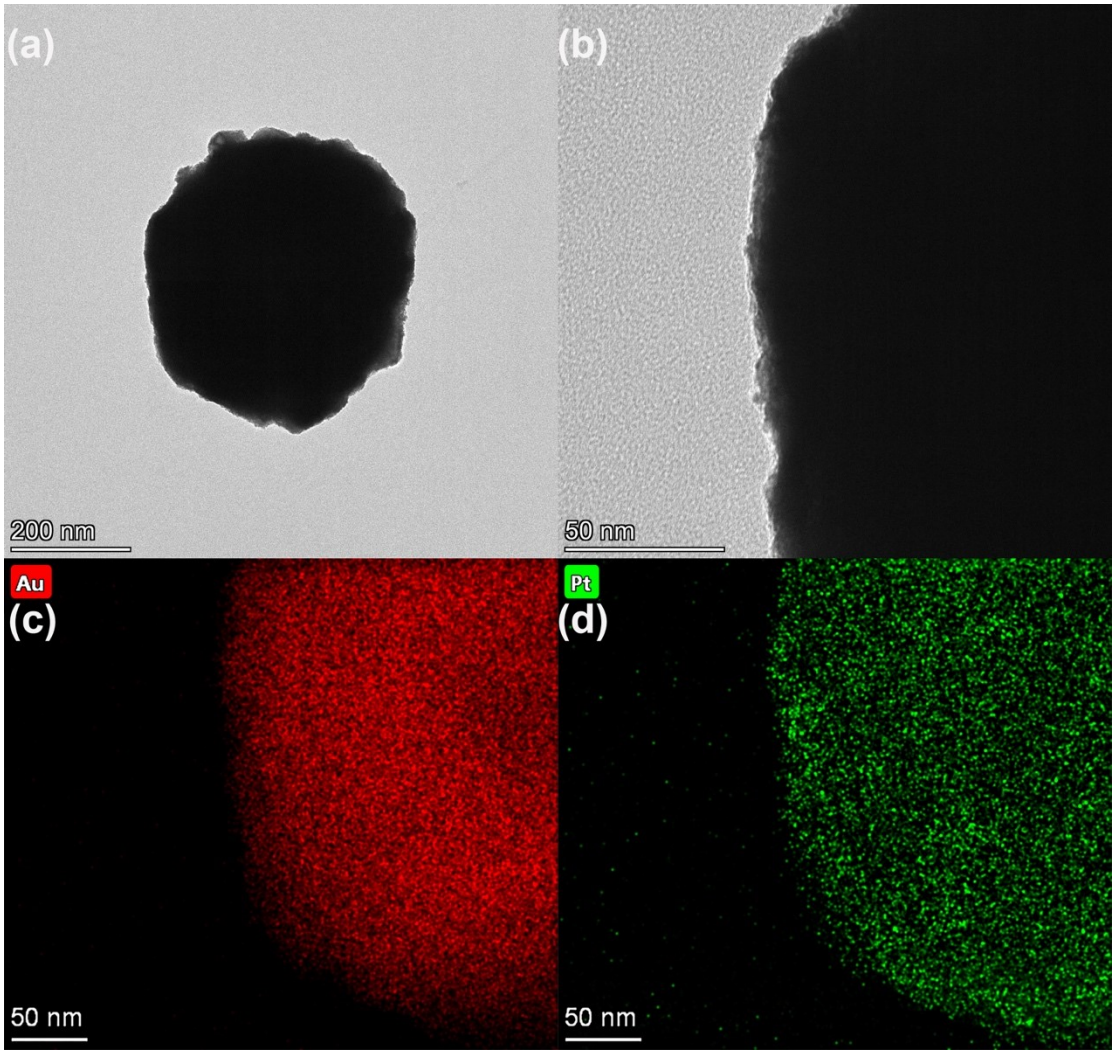

Figure S14. (a) Morphological characterization and (b) magnified image of 2% Pt of AuPt (scale bar: 200 nm; 50 nm). EDS elemental mapping of (c) the Au and (d) Pt elemental distribution (scale bar: 50 nm).

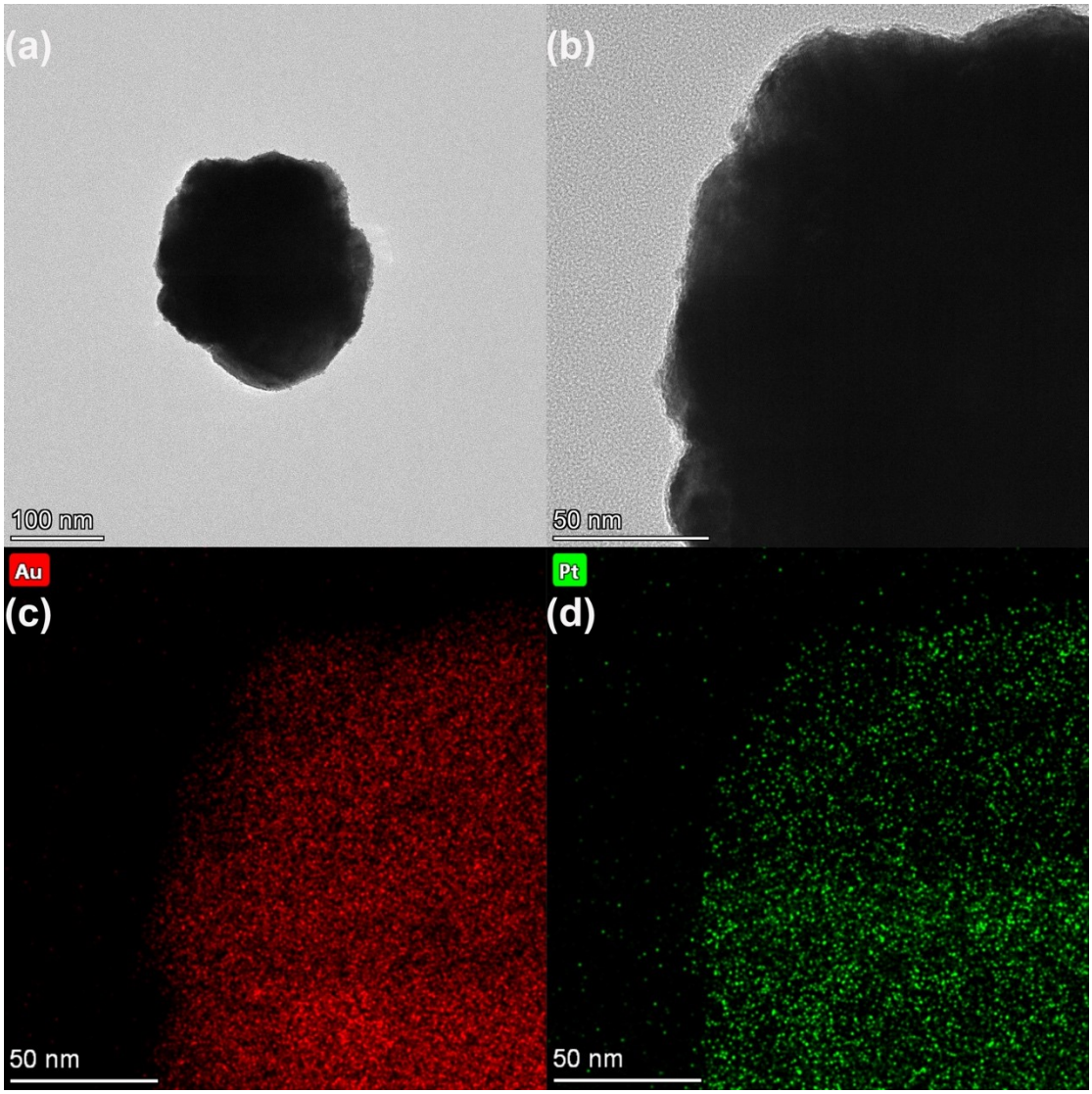

Figure S15. (a) Morphological characterization and (b) magnified image of 3% Pt of AuPt (scale bar: 100 nm; 50 nm). EDS elemental mapping of (c) the Au and (d) Pt elemental distribution (scale bar: 50 nm).

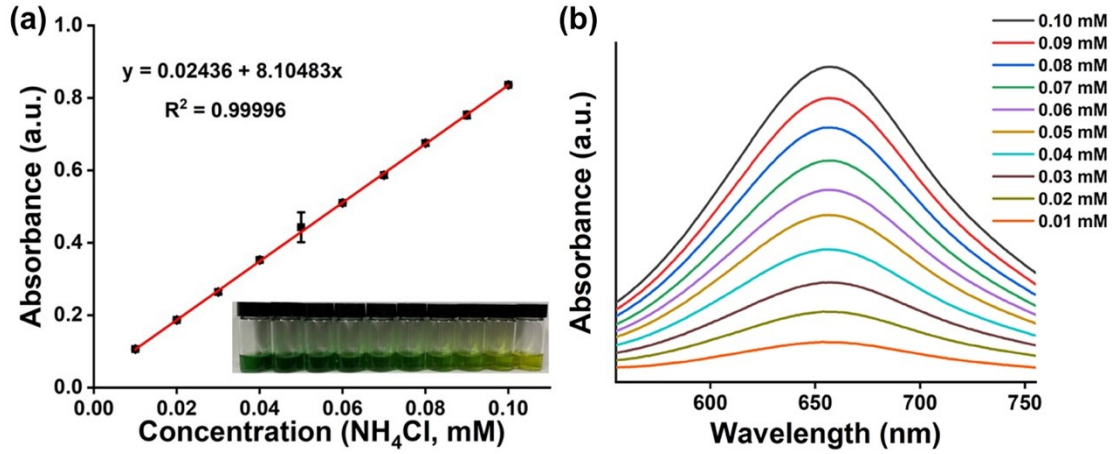

Figure S16. Indophenol blue method for subsequent ammonia quantification. (a) Linear correlation of the absorbance intensity to NH_4^+ concentration. (b) Absorbance spectra of indophenol blue in NH_4^+ solutions at various concentrations.

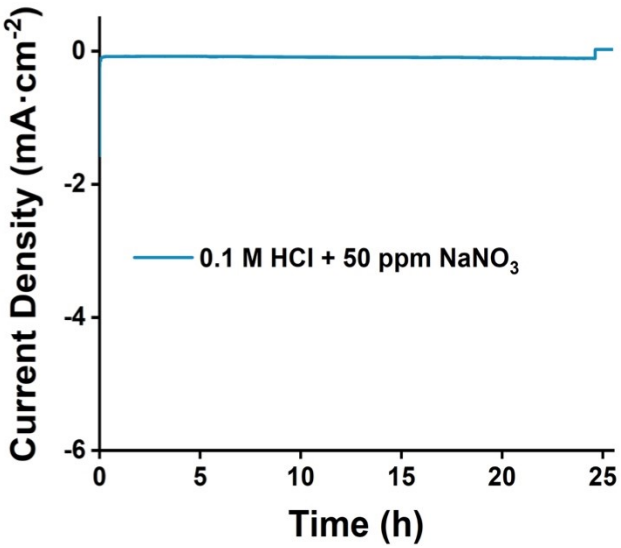

Figure S17 Time-dependent current density for NO_3RR stability at −0.50 V vs RHE in the electrolyte of 0.1 M HCl and 50 ppm $NaNO_3$.

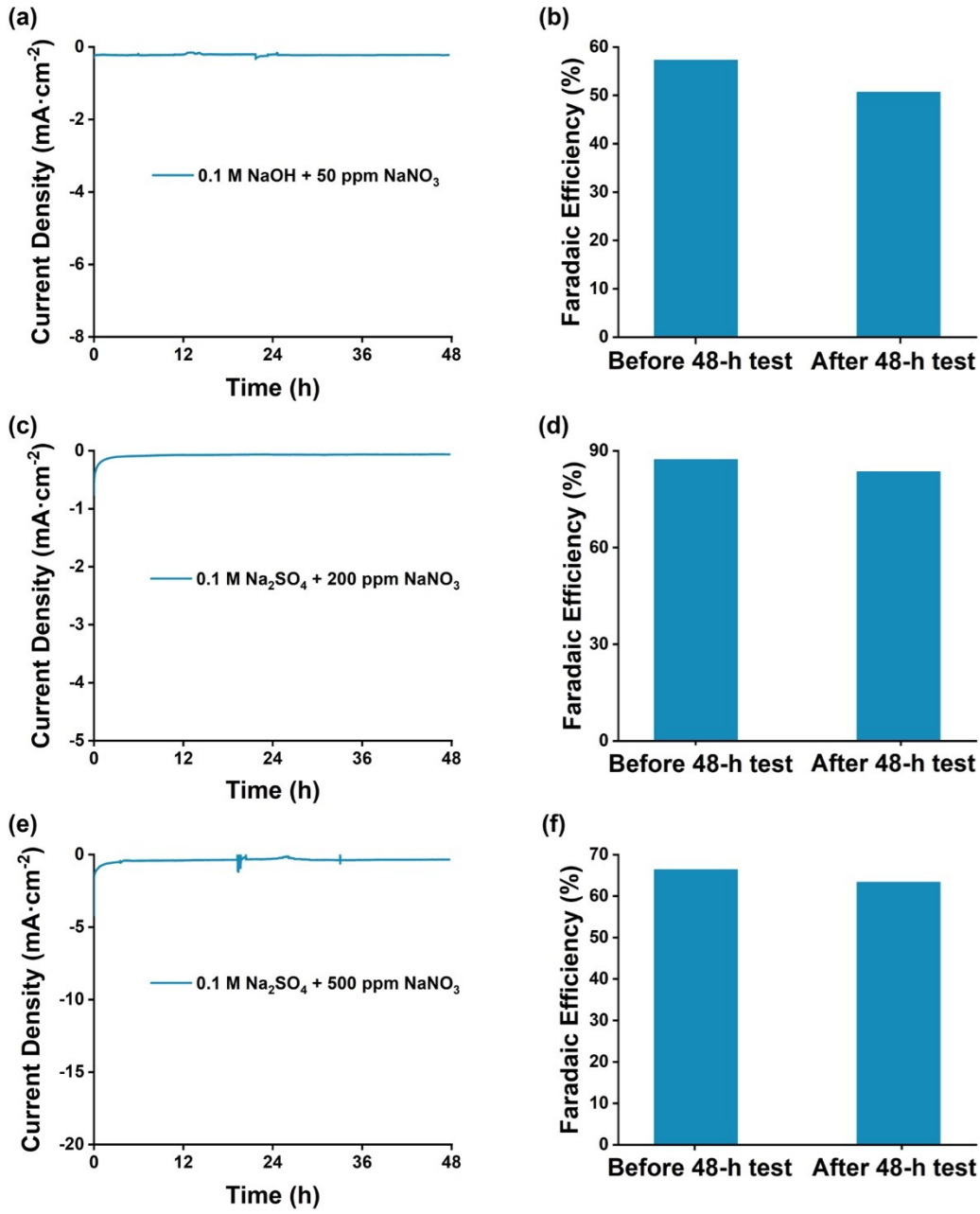

Figure S18. (a) Time-dependent current density for 48-h NO_3RR at −0.50 V vs RHE in 0.1 M NaOH and 50 ppm $NaNO_3$. (b) Comparison of Faradaic efficiency before and after 48-h electrolysis in 0.1 M NaOH and 50 ppm $NaNO_3$. (c) Time-dependent current density for 48-h NO_3RR at −0.50 V vs RHE in 0.1 M Na_2SO_4 and 200 ppm $NaNO_3$. (d) Comparison of Faradaic efficiency before and after 48-h electrolysis in 0.1 M Na_2SO_4 and 200 ppm $NaNO_3$. (e) Time-dependent current density for 48-h NO_3RR at −0.50 V vs RHE in 0.1 M Na_2SO_4 and 500 ppm $NaNO_3$. (f) Comparison of Faradaic efficiency before and after 48-h electrolysis in 0.1 M Na_2SO_4 and 500 ppm $NaNO_3$.

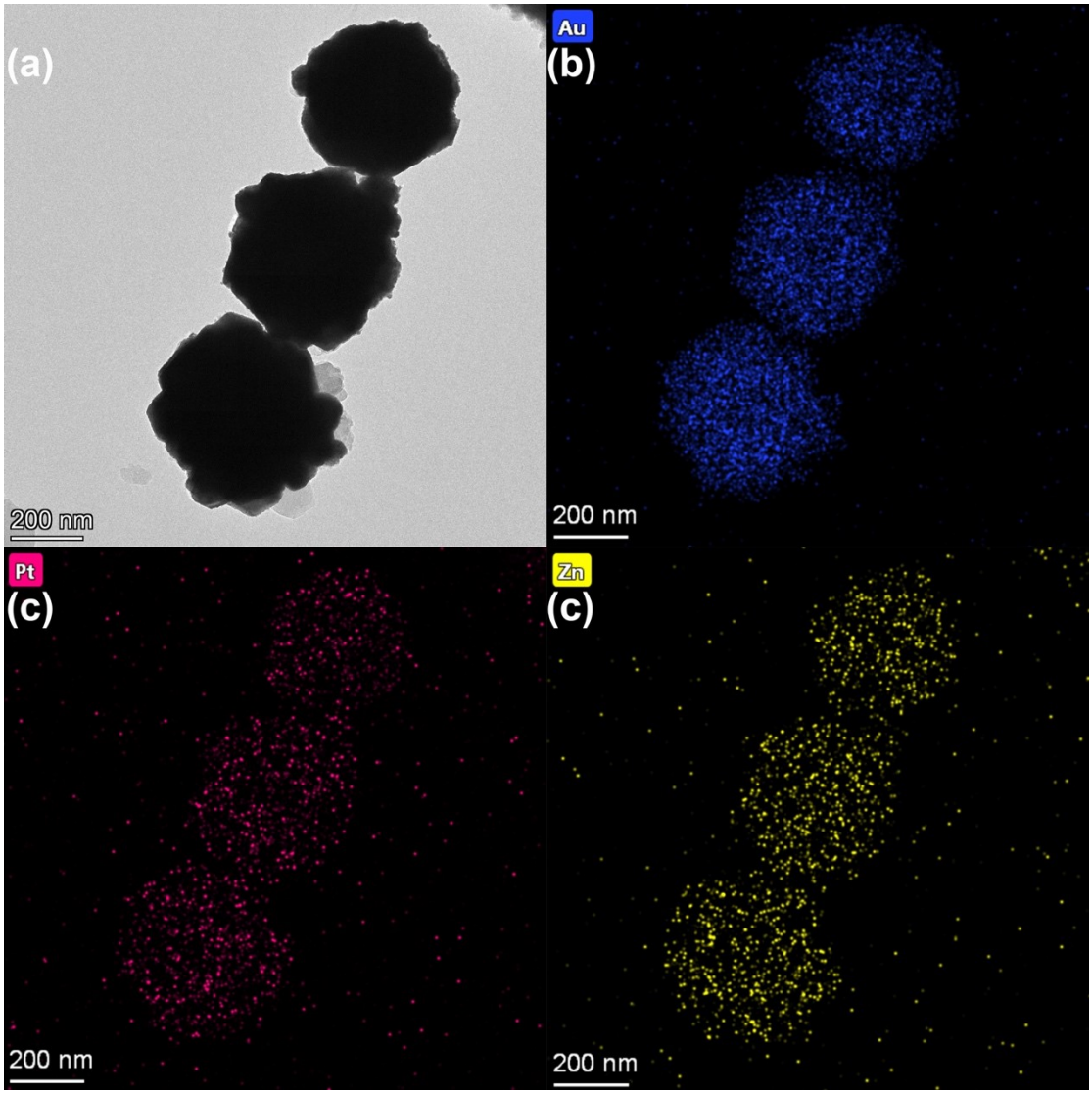

Figure S19. (a) Morphological characterization of the AuPt@ZIF-8 after long-period NO_3RR catalysis in the TEM image. The porous AuPt particles still maintain a spherical morphology and exhibit interconnected pores with no collapsed stucture. EDS elemental mapping of (b) Au, (c) Pt and (d) Zn elements, showing homogeneous distribution.

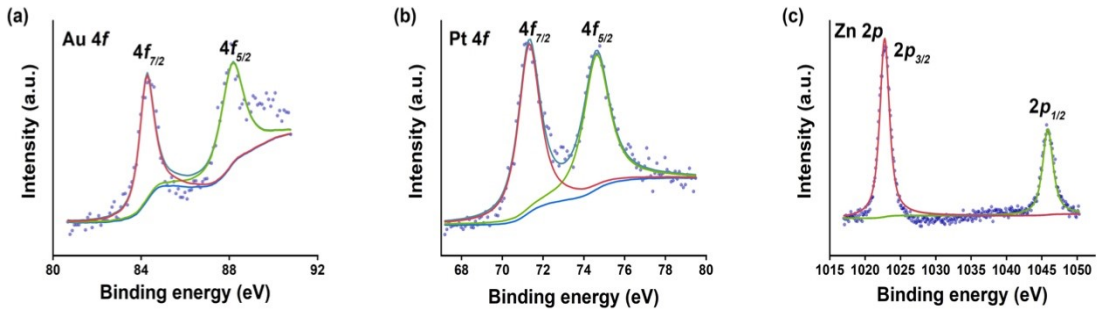

Figure S20 XPS spectra at (a) Au 4*f*, (b) Pt 4*f*, (c) Zn 2*p* binding energy windows for AuPt@ZIF-8 after NO_3RR.

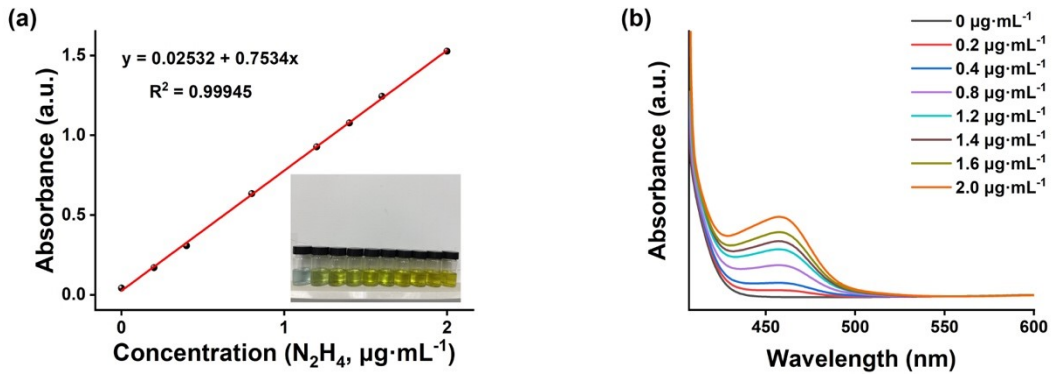

Figure S21. Method for subsequent hydrazine quantification. (a) Calibration curve used for calculation of N_2H_4 concentration. (b) Absorbance spectra of N_2H_4 solutions with various concentrations after incubated for 20 minutes at room temperature.

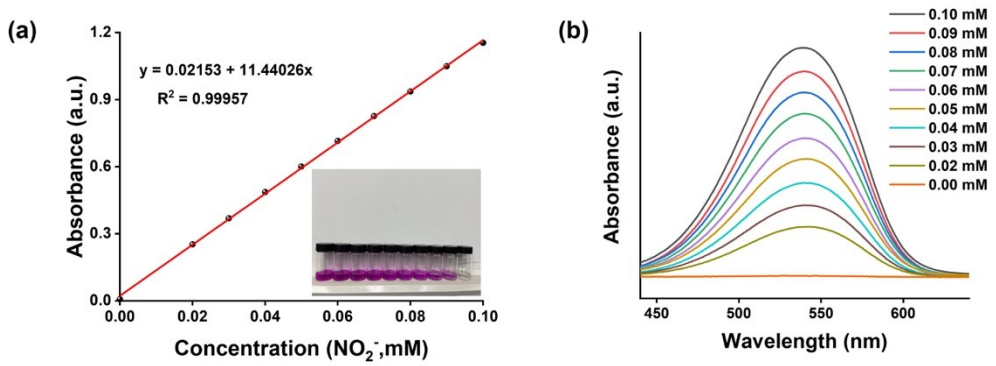

Figure S22. Calibration of UV/Vis spectrophotometry for subsequent NO_2^- quantification. (a) Linear correlation of the absorbance intensity to NO_2^- concentration (inset shows the formation of indophenol blue with different NO_2^- concentrations). (b) Absorbance spectra of UV/Vis spectrophotometry in NO_2^- solutions at various concentrations.

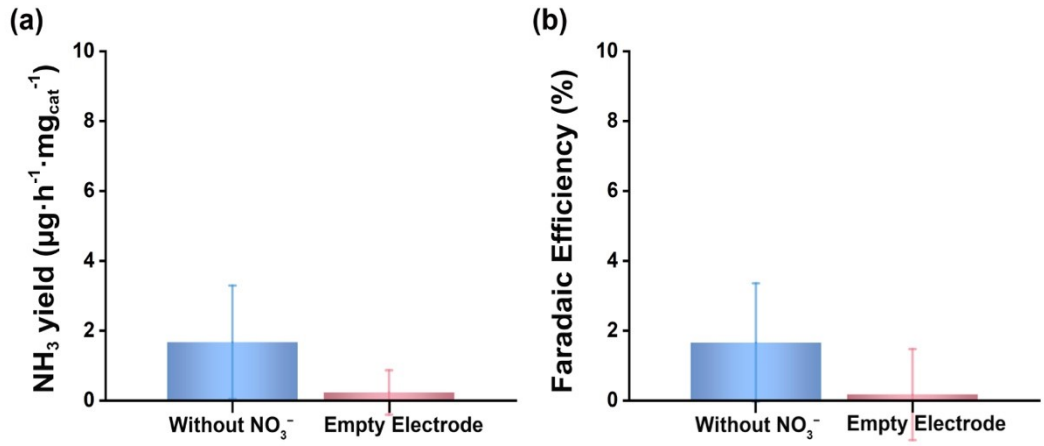

Figure S23. (a) NH_3 yield rate and (b) Faradaic efficiency in the electrolyte without NO_3^- and using blank electrode. The experiment 'without nitrate' exclude the possibility of ammonia contamination from environmental factor, such as the ammonia from the glasswares, environment, labwares, N component in the electrocatalyst. The experiment 'blank electrode' proves that the enhancement of NO_3RR is resulted from the AuPt@ZIF-8 instead of other components.

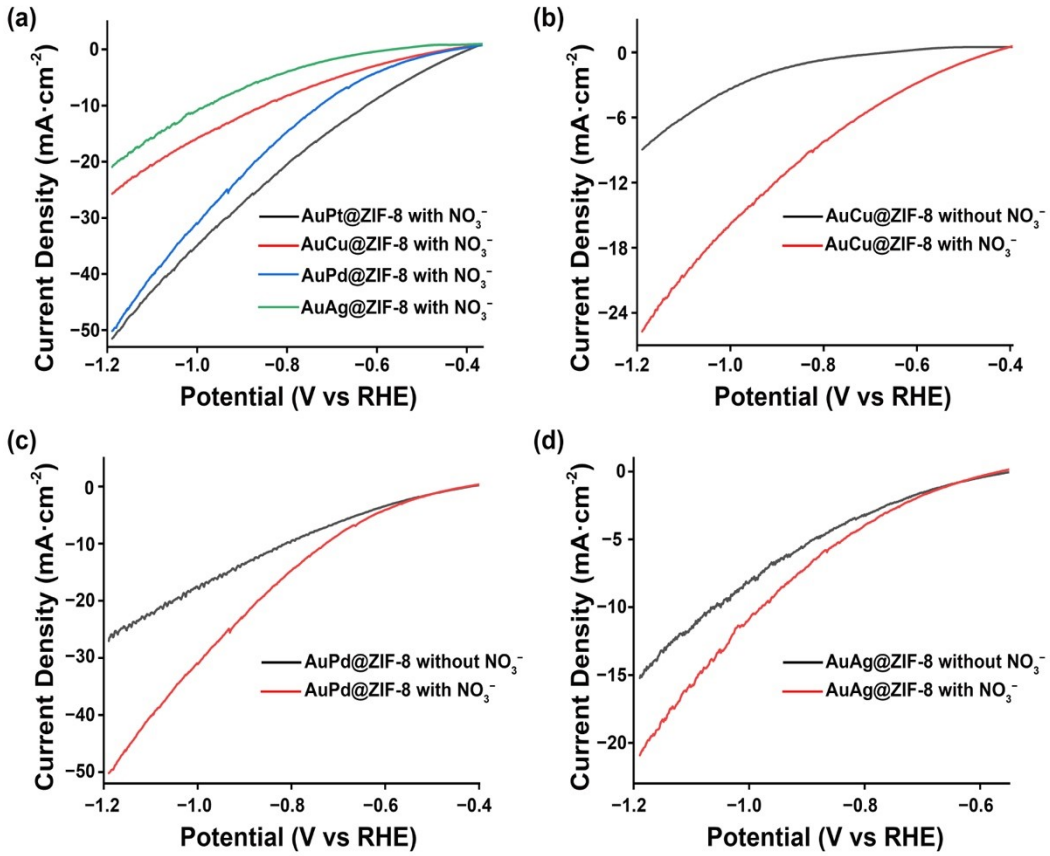

Figure S24. (a) AuPt@ZIF-8, AuCu@ZIF-8, AuPd@ZIF-8, AuAg@ZIF-8 LSV curves under the and with NO_3^- environment. (b) AuCu@ZIF-8 LSV curves under the without NO_3^- and with NO_3^- environment. (c) AuPd@ZIF-8 LSV curves under the without NO_3^- and with NO_3^- environment. (d) AuAg@ZIF-8 LSV curves under the without NO_3^- and with NO_3^- environment. AuPt@ZIF-8 exhibits higher current density in the NO_3^- electrolyte, stating preferable NO_3RR activity.

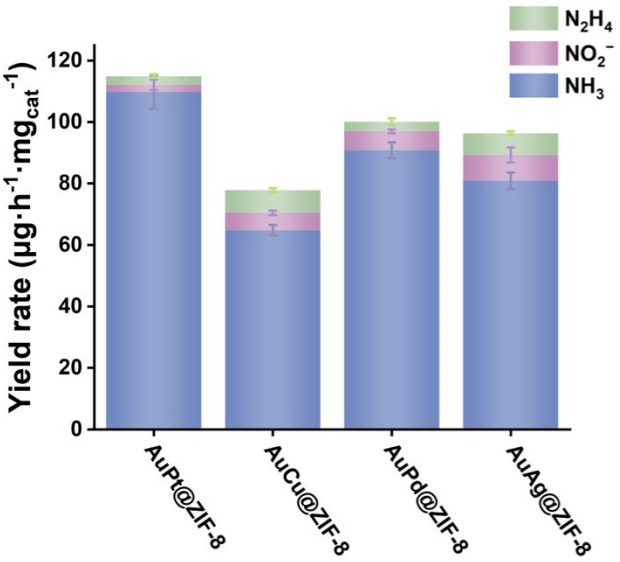

Figure S25. AuPt@ZIF-8, AuCu@ZIF-8, AuPd@ZIF-8, AuAg@ZIF-8 of yield rate for NH_3, NO_2^- and N_2H_4 generated during the NO_3RR at −0.50 V vs RHE.

Table S1 The ammonia yield and faradaic efficiency for different Pt ratios.

Mass ratios of Pt in AuPt@ZIF-8	NH_3 yield ($\mu g \cdot h^{-1} \cdot mg_{cat}^{-1}$)	Faradaic efficiency (%)
1% Pt	52.37	75.11
2% Pt	131.51	95.80
3% Pt	61.91	67.14

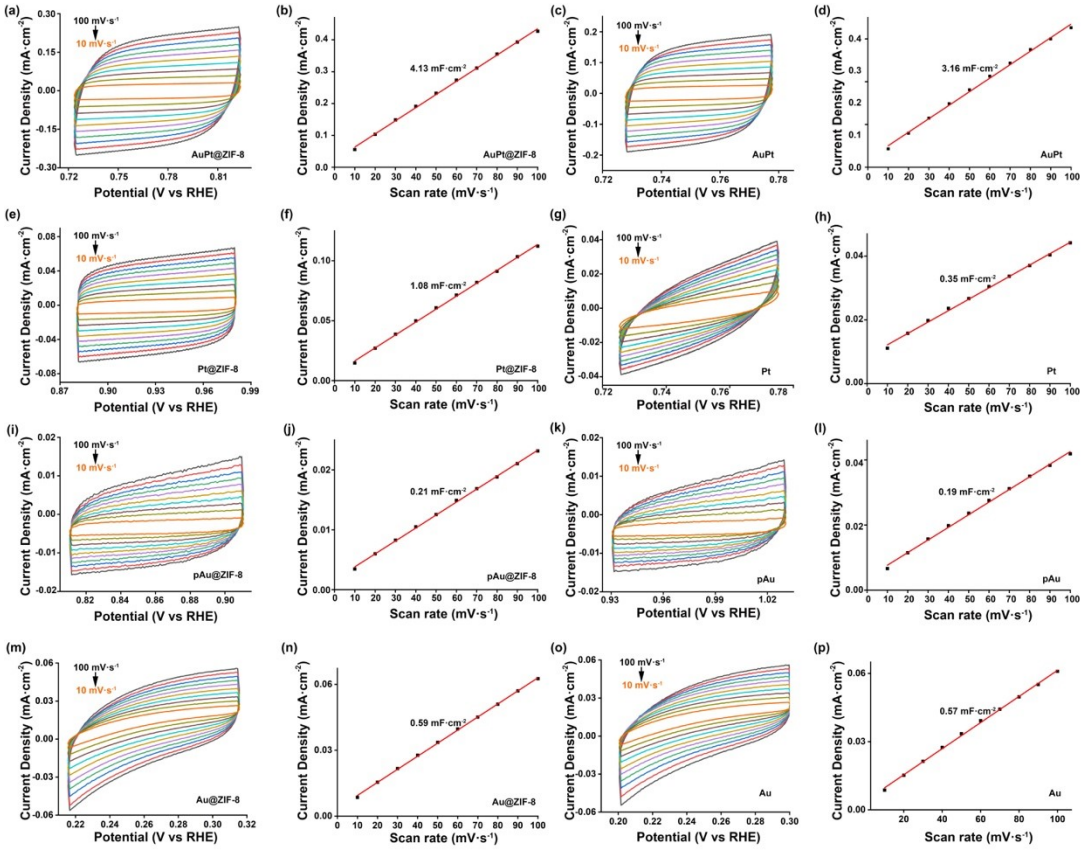

Figure S26 Cyclic voltammetry tests for synthesized (a) AuPt@ZIF-8, (c) AuPt, (e) Pt@ZIF-8, (g) Pt, (i) pAu@ZIF-8, (k) pAu, (m) Au@ZIF-8, (o)Au and (b), (d), (f), (h), (j), (l) (n) (p) charging current density differences plotted against scan rates, respectively. The C_{dl} value for AuPt@ZIF-8 is 4.13 mF·cm^{-2}, higher than that for AuPt, Pt@ZIF-8, Pt, pAu@ZIF-8, pAu, Au, Au@ZIF-8 (3.16, 1.08, 0.35, 0.21, 0.19, 0.57, 0.59 mF·cm^{-2}).